US National Oceanic and Atmospheric Administration
Climate Test Bed Joint Seminar Series
ESSIC/UMD, College Park, Maryland, 10 May 2010

Variability and Prediction of the Asian and Indo-Pacific Monsoon Climate in the NCEP Climate Forecast System

Song Yang

Climate Prediction Center, NOAA/NWS/NCEP
Camp Springs, MD, 20746

1. Introduction

The NCEP Climate Forecast System (CFS) is one of the state-of-the-art global models that have been applied to understand and predict the variability of global climate. It is one of the important tools for the official forecasts of U.S. monthly and seasonal temperature and precipitation at the NOAA Climate Prediction Center. CFS products are also becoming an important source of information for regional climate predictions in many countries outside the U.S.

In this presentation, a comprehensive review of the characteristics of monsoon climate over the Asian and Indo-Pacific sector in the NCEP CFS and the skill of monsoon prediction by the system is provided. Particular emphasis is placed on the impacts of El Niño-Southern Oscillation (ENSO), Indian Ocean (IO) sea surface temperature (SST), land surface process, ocean-atmosphere coupling, and model resolutions. Results from model evaluation by advanced tools are also discussed.

The presentation is based on the results from the studies of Yoo *et al.* (2006), Yang *et al.* (2008a, b), Liang *et al.* (2009), Gao *et al.* (2010), Li and Yang (2010), Yang *et al.* (2010), and Yoo *et al.* (2010). The model output analyzed includes the following products: (1) 15-member retrospective prediction runs of the CFS, an operational version in resolution T62, (2) a set of 10-member hindcasts of the CFS in T126 for different land models and land initial conditions, and (3) free runs of the model in both T62 and T126. The above studies also employ the following (re)analysis and observational data sets: the NCEP-NCAR reanalysis, CPC CMAP precipitation, NOAA SST, and CPC surface temperature analysis.

2. Results

(a) Summer monsoon

For the Asian summer monsoon, several major features have been revealed:

(i) Figure 1 shows the summer climatology of CMAP precipitation, CFS precipitation, and their difference. Figure 1a illustrates several centers of observed precipitation over western India, Bangladesh-Burma, Indo-China peninsula, South China Sea, and east of the Philippines, with the highest center over Bangladesh, Burma, and northern Bay of Bengal. It also shows large precipitation over the tropical central-eastern IO and the Meiyu rain band over eastern China, Baiu over Japan, and Changma over Korea. Furthermore, the figure shows relatively lighter precipitation over the eastern Indian coast, east of Indo-China peninsula, and the northwestern Pacific. Light precipitation is also seen over the western

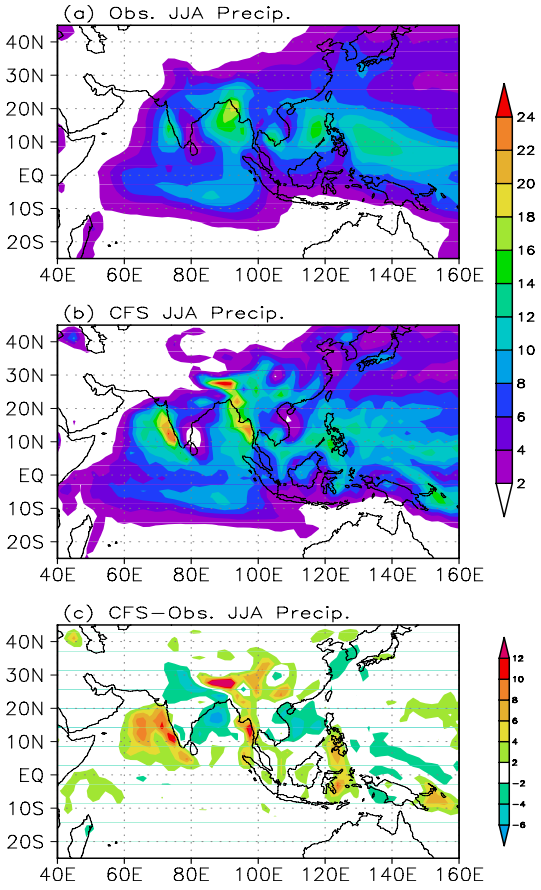

Fig. 1 Fig. 1. (a) 1981-2003 climatology of JJA precipitation from CMAP, (b) 1981-2003 climatology of JJA ensemble-mean precipitation from CFS T62 (zero month lead), and (c) difference between (b) and (a). Units: mm per day.

Correspondence to: Song Yang, Climate Prediction Center, NOAA/NWS/NCEP, Camp Springs, MD, 20746;
E-mail: Song.Yang@noaa.gov

Arabian Sea where ocean upwelling driven by monsoon flow cools the sea surface. Comparison between Figs. 1a and 1b indicates that the CFS captures the general features of observed precipitation quite well. For example, the model captures the locations of major high and low centers of monsoon precipitation. The model precipitation and observed precipitation also compare reasonably well in magnitude in many places. A merit of the CFS appears in simulating the East Asian Meiyu rain band and the precipitation over the tropical IO. In particular, while general circulation models often fail to produce the Meiyu rain band, the CFS captures the phenomenon of precipitation reasonably well, in spite of an underestimation of precipitation over Korea and the Yellow Sea. The CFS performs well in capturing the tropical IO precipitation center, for which many models even fail in reproducing the shape of the precipitation center. However, the CFS overestimates the precipitation over the eastern Arabian Sea, the Himalayas, and Burma, and underestimates the precipitation over northwestern Bay of Bengal, northern India, and South China Sea (see Fig. 1c). The overestimation of precipitation over the southern-southeastern hills of the Tibetan plateau seems one of the main problems of monsoon simulations by the model.

(ii) The skill of prediction of several dynamical monsoon indices can be seen from Fig. 2. The CFS is highly skillful in predicting the large-scale Asian summer monsoon circulation, as seen in the confidence of predicting the monsoon measured by the Webster-Yang monsoon index (Webster and Yang 1992), which exceeds the 99% confidence level (R=0.52; Student *t*-test) using the initial conditions (ICs) of January (4 months lead (LM4)) and the 95% level (R=0.41) using the ICs of December (LM5). The Southeast Asian monsoon (measured by Goswami *et al.* 1999) can be predicted at the 99% confidence level using the ICs of April and at the 95% confidence level using the ICs of March. In addition, the South Asian monsoon (measured by Wang and Fan 1999) is also predictable at the 95% confidence level using the ICs of April. However, no skill is found in predicting the East Asian monsoon (measured by Lau *et al.* 2000).

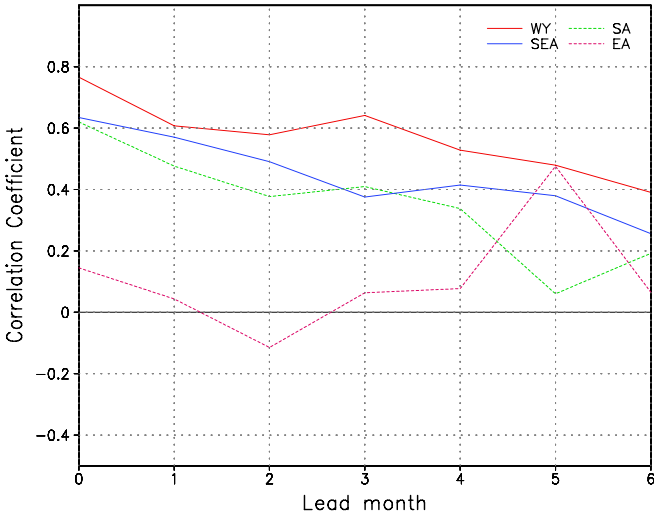

Fig. 2 The coefficients of correlation between the CFS T62 predicted and observed monsoons for different lead months. Values are shown for different dynamical monsoon indices.

(iii) It is found that the skill of monsoon prediction by the CFS comes mainly from the impact of ENSO. The most predictable patterns of monsoon rainfall depicted by the empirical orthogonal function (EOF) analysis with maximum signal-to-noise ratio (MSN) exhibit many features that are seen from the rainfall anomalies associated with the influence of ENSO. Nevertheless, the ENSO-monsoon relationship in the CFS is stronger than that observed. As observed, there are apparent relationships between the various monsoon components and IO SST especially the SST over southern IO. However, these relationships disappear or become much weaker in AMIP experiments in which the atmosphere and oceans are not coupled.

(iv) Figures 3a-c show the climatological patterns of observed summer precipitation and 850-mb winds and the difference in precipitation and winds between CFS T62 and observations. Over the Asian continent, the CFS T62 has difficulties in simulating the precipitation near the Tibetan plateau (Fig. 3b). It underestimates the precipitation over northern India and overestimates the precipitation over western China. These problems become less serious in T126 than in T62 (compared Fig. 3b and Fig. 3c). More apparent improvement in precipitation and atmospheric circulation simulations from T62 to T126 can be found for September-November (Figs. 3d-f). Figures 3e-f indicates an improvement in SON precipitation simulation over western and eastern Asia including India and China. The largest improvement occurs over the tropical Indian Ocean. For example, the CFS T62 has difficulty in simulating the climatological zonal dipole structure and its associated atmospheric circulation near the equator. In T126, the dipole structure has been simulated much more realistically, as reflected by the smaller model-observation differences in precipitation and winds.

These results suggest a better simulation of the Asian summer monsoon by the next generation of the CFS whose atmospheric component has a horizontal resolution of T126. The apparent improvement in simulating the Asian monsoon from T62 to T126 is in a sharp contrast to the simulation of the North American monsoon in which little improvement is seen from T62 to T126 for the monsoon rainfall over Southwest U.S. (Yang *et al.* 2009).

(v) In spite of the high skill of the CFS in simulating and predicting the variations (anomalies) of the large-scale patterns of the Asian monsoon, a weak bias can be clearly seen. We attribute the weak monsoon circulation in the CFS to the cold bias in the model over the much of the Asian continent, which causes a weaker-than-observed thermal contrast between the continent and oceans. As shown in Fig. 4, several experiments using CFS T126 with the current 2-level Oregon State University land model and the advanced 4-level Noah land model indicate a clear improvement. For example, the cold bias over the Asian continent is significantly reduced in the experiment using the Noah model, leading to improvements in temperature and precipitation simulations. The result suggests a better simulation of the Asian summer monsoon by the next generation of the CFS in which the Noah land model is used. (It should be pointed out that the difference between the land ICs from NCEP-DOE global reanalysis II (R2) and those from the Global Land Data Assimilation System (GLDAS) is usually small.)

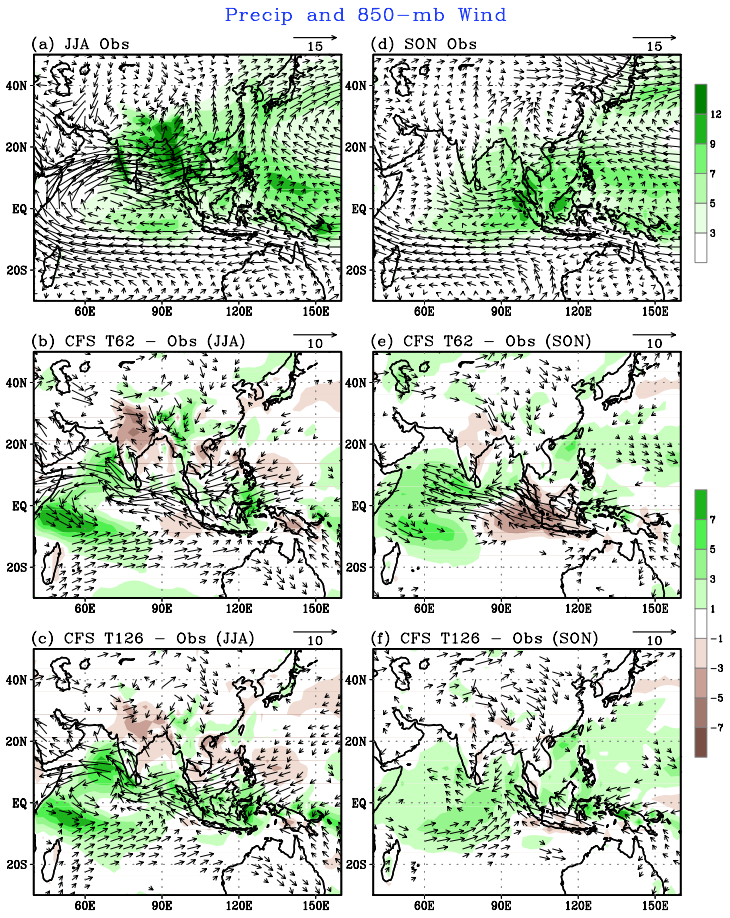

Fig. 3 1951-2005 climatological patterns of precipitation and 850-winds (NCEP-NCAR reanalysis) for JJA (a) and SON (d). (b) and (e): Differences in precipitation and winds between CFS T62 and observations. (c) and (f): Differences in precipitation and winds between CFS T126 and observations. The climatologies of 45 years are used for CFS.

(b) Winter monsoon

The East Asian winter monsoon appears prominently not only at the lower troposphere but also at the upper troposphere. It interacts with both extratropical and tropical processes. We thus define a new dynamical monsoon index so that it links to the monsoon-related atmospheric systems or parameters at both lower and upper troposphere and is able to depict the association of the monsoon with the Arctic Oscillation and ENSO. In both observations and the CFS, the index is strongly associated with the Siberian high, the East Asian trough, the East Asian and northwestern jet stream, and the lower-tropospheric meridional wind and air temperature over East Asia (Fig. 5 and figures not shown here). It is significantly related to the first EOF modes of the respective fields including sea level pressure, 500-mb height, 200-mb zonal wind, 850-mb meridional wind, and surface air temperature. The CFS can predict the newly-defined winter monsoon index in advance by 4 months, using the ICs in August, with a reasonable skill. A comparison of this index with several major previous indices used commonly indicates that the new index is most predictable, in term of the highest skill and the longest lead time.

(c) East Asian Mei-yu

Here, we focus on the Mei-yu over China, Baiu over Japan, and Changma over Korea during June-July and refer to them as East Asian Mei-yu (EAMY). Compared to the tropical monsoons, the subtropical-extratropical EAMY is relatively less predictable and the studies of the climatic characteristics of EAMY are largely infrequent.

Despite that climate models face tremendous difficulties in simulating and predicting EAMY, the NCEP CFS has demonstrated skill in capturing the Mei-yu rain bands and many large-scale features associated with EAMY. In both observations and the CFS, the EAMY is strongly associated with ENSO, subtropical northwestern Pacific high, and large-scale water vapor transport. As for tropical monsoons, air-sea interaction is important for simulating and predicting EAMY, as indicated by a comparison between the CFS hindcast and uncoupled AMIP experiments with the CFS atmospheric model. A maximum signal-to-noisy EOF analysis shows that the EAMY is the most predictable mid-summer rainfall pattern of the East Asian summer monsoon system (see Fig. 6). It is also shown that the CFS can predict the June-July EAMY in advance by one month with the ICs in May with a reasonable skill.

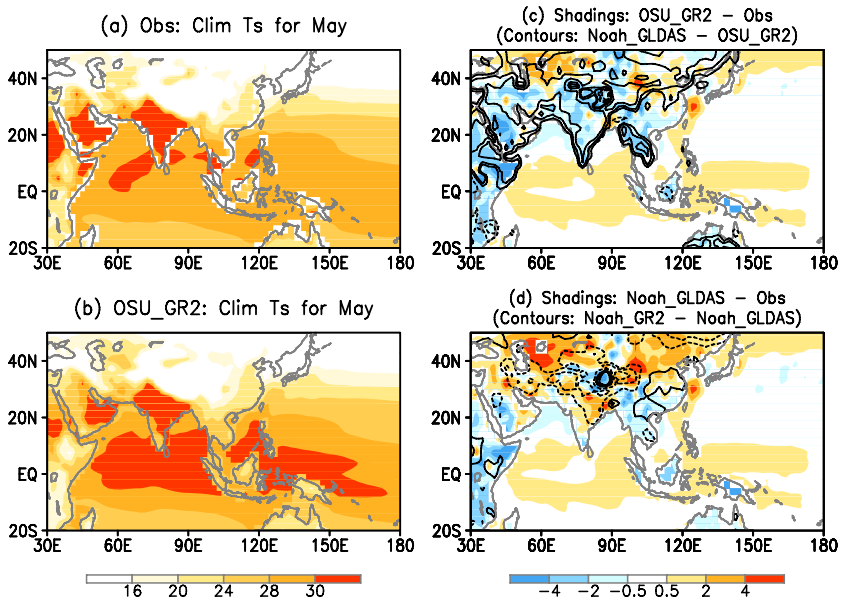

Fig. 4 Climatological patterns of May SST and surface air temperature over lands (ºC) for (a) observations, (b) OSU_GR2, and (c-d) the differences in temperature between observations and CFS output. The shadings in (c) measure the difference between observations and OSU_GR2 and those in (d) measure the difference between observations and Noah_GLDAS. The contours in (c) are for the difference between Noah_GLDAS and OSU_GR2 and those in (d) for the difference between Noah_GR2 and Noah_GLDAS (contour levels: -2, -1, -0.5, 0.5, 1, and 2).

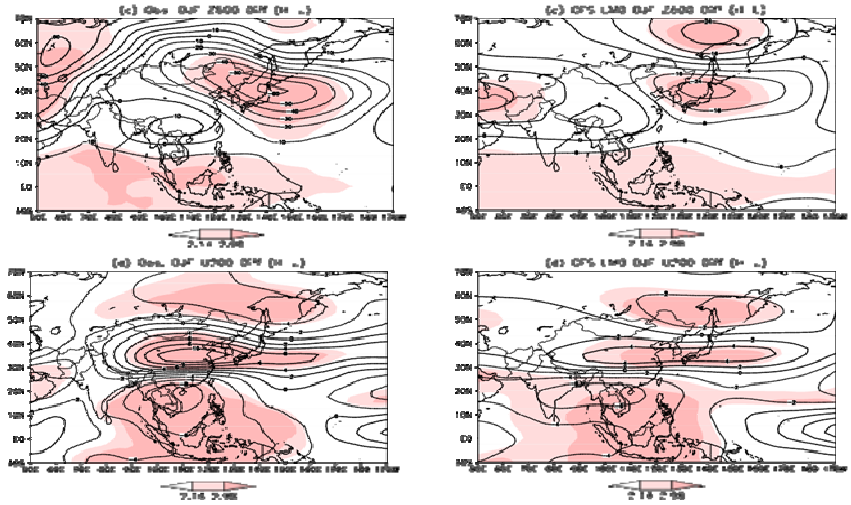

Fig. 5 Composite differences in observed 500-mb geopotential height (a) and 200-mb zonal wind (b) between high values and low values of the newly-define East Asian winter monsoon index. (c) and (d) are the as in (a) and (b), but for the NCEP CFS.

References

Gao, H., S, Yang, A. Kumar, Z.-Z. Hu, B. Huang, Y. Li, and B. Jha, 2010: Variability of the East Asian Meiyu and simulation and prediction by the NCEP Climate Forecast System. *J. Climate*, conditionally accepted.

Goswami, B. N., B. Krishnamurthy, and H. Annamalai, 1999: A broad-scale circulation index for interannual variability of the Indian summer monsoon. *Quart. J. Roy. Meteor. Soc.*, **125**, 611-633.

Lau, K.-M., K.-M. Kim, and S. Yang, 2000: Dynamical and boundary forcing characteristics of regional components of the Asian summer monsoon. *J. Climate*, **13,** 2461-2482.

Li, Y., and S. Yang, 2010: A dynamical index for the East Asian winter monsoon. *J. Climate*, in press.

Liang, J., S. Yang, Z.-Z. Hu, B. Huang, A. Kumar, and Z. Zhang, 2009: Predictable patterns of Asian and Indo-Pacific summer precipitation in the NCEP CFS. *Climate Dynamics*, **32,** 989-1001.

Wang, B., and Fan, Z., 1999: Choice of South Asian monsoon indices. *Bull. Amer. Meteor. Soc*., **80**, 629-638.

Webster, P. J., and S. Yang, 1992: Monsoon and ENSO: Selectively interactive systems. *Quart. J. Roy. Meteor. Soc.*, **118,** 877-926.

Yang, S., M. Wen, and R. W. Higgins, 2008a: Sub-seasonal features of the Asian summer monsoon in the NCEP Climate Forecast System. *ACTA Oceanologica Sinica*, **27,** 88-103.

Yang, S., Z. Zhang, V. E. Kousky, R. W. Higgins, S.-H. Yoo, J. Liang, and Y. Fan, 2008b: Simulations and seasonal prediction of the Asian summer monsoon in the NCEP Climate Forecast System. *J. Climate*, **21,** 3755-3775.

Yang, S., Y. Jiang, D. Zheng, R. W. Higgins, Q. Zhang, V. E. Kousky, and M. Wen, 2009: Variations of U.S. regional precipitation and simulations by the NCEP CFS: Focus on the Southwest. *J. Climate*, **22,** 3211-3231.

Yang, S., M. Wen, R. Yang, K. E. Mitchell, R. W. Higgins, and J. Meng, 2010: Impacts of land surface models and land surface initial conditions on the onset of Asian summer monsoon in the NCEP CFS. *J. Hydrometeor.*, to be submitted.

Yoo, S.-H., S. Yang, and C.-H. Ho, 2006: Variability of the Indian Ocean sea surface temperature and its impacts on Asian-Australian monsoon climate. *J. Geophys. Res.*, **111,** D03108, doi:10.1029/2005JD006001.

Yoo, S.-H., J. Fasullo, S. Yang, and C.-H. Ho, 2010: Relationship between Indian Ocean SST and the transition from El Niño to La Niña. *J. Geophys. Res.*, in press.

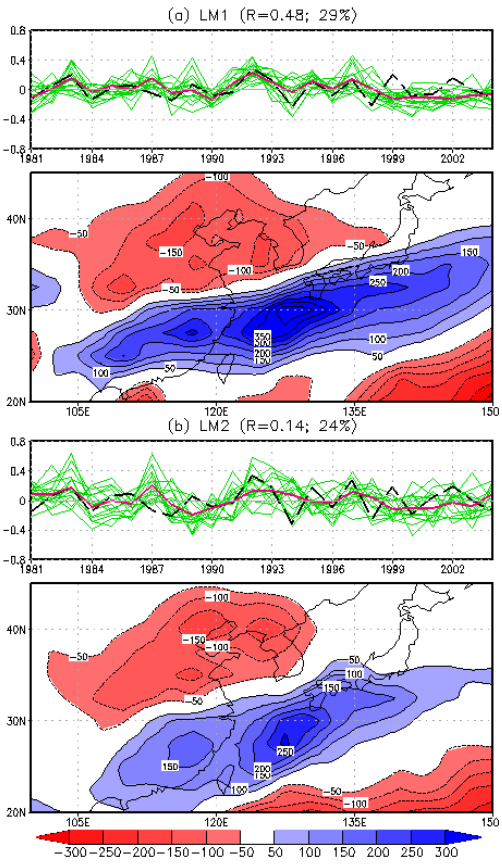

Fig. 6 First MSN EOF mode of the CFS EAMY precipitation (mm) for LM1 (a) and LM2 (b) and the corresponding time series. For the time series, thick red and thin green lines are the PCs of ensemble means and individual members, respectively. The thick black lines represent the PCs computed by projecting the observed precipitation upon the pattern of the first mode of CFS precipitation. R measures the correlation between the observation and the ensemble mean. Contour interval is 50.